C2 SMART
CONNECTED CITIES WITH SMART TRANSPORTATION

A USDOT University Transportation Center

New York University

Rutgers University

University of Washington

The University of Texas at El Paso

City College of New York

Field Application of a High-Power Density Electromagnetic Energy Harvester to Power Wireless Sensors in Transportation Infrastructures

May 2023

TECHNICAL REPORT DOCUMENTATION PAGE

1. Report No.	2. Government Accession No.	3. Recipient's Catalog No.	
4. Title and Subtitle Field Application of a High-Power Density Electromagnetic Energy Harvester to Power Wireless Sensors in Transportation Infrastructures		5. Report Date May 2023	
		6. Performing Organization Code:	
7. Author(s) Anil Agrawal, Mohsen Amjadian, Wai Yan Tun, Hani Nassif, Hongfan Wang		8. Performing Organization Report No.	
9. Performing Organization Name and Address Connected Cities for Smart Mobility towards Accessible and Resilient Transportation Center (C2SMART), 6 Metrotech Center, 4th Floor, NYU Tandon School of Engineering, Brooklyn, NY, 11201, United States		10. Work Unit No.	
		11. Contract or Grant No. 69A3551747119	
12. Sponsoring Agency Name and Address Office of Research, Development, and Technology Federal Highway Administration 6300 Georgetown Pike McLean, VA 22101-2296		13. Type of Report and Period Final Report, 3/1/2022 - 4/30/2023	
		14. Sponsoring Agency Code	
15. Supplementary Notes			

16. Abstract

Finding an efficient source of energy has always been a big challenge for humans on Earth. Fossil fuels, such as coal and oil, have traditionally been considered as major sources of energy. These energy sources are not only nonrenewable but are also harmful to our health and environment. A large portion of this energy is consumed by vehicles moving daily in big cities, causing significant pollution of the environment.

However, the motion of vehicles through the transportation infrastructures can also be a significant source of kinetic energy, which can be harvested to power transportation system components, such as sensors, street lights, signals, etc., thereby reducing some dependence on fossil fuel-derived energy.

17. Key Words		18. Distribution Statement No restrictions. This document is available to the public through the National Technical Information Service, Springfield, VA 22161. http://www.ntis.gov		
19. Security Classif. (of this report) Unclassified		20. Security Classif. (of this page) Unclassified	21. No. of Pages 42	22. Price

Form DOT F 1700.7 (8-72)   Reproduction of completed page author

Harvesting Electric Energy from Traffic-Induced Vibration of Transportation Infrastructures to Power Wireless Sensors: Field Application of A High-Power Density Electromagnetic Energy Harvester

Dr. Anil Agrawal
The City College of New York
0000-0001-6660-2299

Dr. Mohsen Amjadian
The University of Texas Rio Grande Valley
Rio Grande Valley 0000-0002-6786-8707

Wai Yan Tun
The University of Texas
0000-0003-1753-3738

Dr. Hani Nassif
Rutgers University
0000-0002-3441-3589

Hongfan Wang
The City College of New York
0000-0001-6854-511X

C2SMART Center is a USDOT Tier 1 University Transportation Center taking on some of today's most pressing urban mobility challenges. Some of the areas C2SMART focuses on include:

Urban Mobility and Connected Citizens

Urban Analytics for Smart Cities

Disruptive Technologies and their impacts on transportation systems. Our aim is to develop innovative solutions to accelerate technology transfer from the research phase to the real world.

Unconventional Big Data Applications from field tests and non-traditional sensing technologies for decision-makers to address a wide range of urban and mobility problems with the best information available.

Impactful Engagement overcoming institutional barriers to innovation to hear and meet the needs of city and state stakeholders, including government agencies, policy makers, the private sector, non-profit organizations, and entrepreneurs.

Forward-thinking Training and Development dedicated to training the workforce of tomorrow to deal with new mobility problems in ways that are Urban Analytics for not covered in existing transportation curricula.

Disclaimer

The contents of this report reflect the views of the authors, who are responsible for the facts and the accuracy of the information presented herein. This document is disseminated in the interest of information exchange. The report is funded, partially or entirely, by a grant from the U.S. Department of Transportation's University Transportation Centers Program. However, the U.S. Government assumes no liability for the contents or use thereof.

Acknowledgement

The vibration caused by traffic on transportation infrastructures can be a valuable source of kinetic energy, which can be harvested to power monitoring sensors and peripherals on bridges. This approach not only reduces the reliance on non-renewable energy sources but also taps into an immense source of untapped kinetic energy in the US transportation network, which sees over 5 billion vehicle miles traveled per day. The current study focuses on developing a high-power density electromagnetic energy harvester (EMEH) that can convert this kinetic energy into electrical energy to power sensors installed on transportation infrastructures. The EMEH design, created through analytical and finite element simulations, employs linear arrays of small permanent magnets to achieve a strong and focused magnetic field in a specific orientation. The compact design of the EMEH allows it to be seamlessly integrated into the power circuit of wireless sensor nodes (WSNs) and installed in transportation infrastructures without complicated wiring. It can continuously charge the rechargeable battery of a WSN, thereby extending the lifespan of the monitoring system. This project involves the development and field implementation of a more compact version of the EMEH that the authors developed in the first phase of the research that had only one resonator with two planar arrays of permanent magnets (PMs).

The EMEH developed in this project consists of two resonators and three linear arrays of PMs. A prototype of proposed dual-resonator EMEH (DR-EMEH) is tested under harmonic excitations for a wide range of frequencies. Next, it is installed on selected transportation infrastructures (highway bridges) for testing its energy harvesting efficiency and capability to power various monitoring sensors and peripherals. The study focuses on three different highway bridges with different fundamental frequencies, ideally between 2Hz to 8Hz, and will record the traffic induced vibration of each bridge during normal daily traffic. The EMEH's dynamic characteristics, such as tip mass and spring stiffness (cantilever beams lengths), will be modified to resonate with the bridge by matching their natural frequencies. The study aims to demonstrate the feasibility of the proposed DR-EMEH to power sensors that regularly monitor the structural integrity of materials and components of highway bridges, such as acceleration and temperature sensors.

Table of Contents

List of Tables

Subsection 1.1 Introduction

Fossil fuels such as coal and petroleum are the primary sources of energy. They are, however, nonrenewable, and more importantly harmful to our health and environment when being converted to motion energy. A large portion of fossil fuel-derived energy is consumed by vehicles moving daily in urban areas which is one of the major sources of air pollutants. The motion of vehicles is, however, a significant source of kinetic energy that can be harvested to power sensors and electrical equipment installed on highway bridges for structural health monitoring, thereby reducing some dependence on fossil fuel-derived energy. This reduces the cost of structural health monitoring by eliminating wiring requirements for an external power outlet (Roundy et al., 2004; Williams and Yates, 1996).

There are three different types of energy harvesters typically used to harvest electric power from traffic induced-vibration which are: electromagnetic, piezoelectric, and electrostatic (Priya and Inman, 2009; Roundy et al., 2004). Electromagnetic energy harvesters (EMEHs) are more reliable among them because they do not require mechanical contact between any components. For this reason the effects of wear and tear is minimal in EMEHs, which can reduce the unwanted mechanical damping in the harvester. The basic mechanism of an EMEH is based on the Faraday's law of induction (Khaligh et al., 2010; Wei and Jing, 2017). The relative motion between a permanent magnet (PM) and a conductive medium (e.g. copper coil) causes a change in the magnetic flux of the PM passing through the conductive medium. This change induces the

socalled eddy current inside the conductive medium and the direction of this electric current opposes the change in the external magnetic flux because of the relative motion of the PM and the conductive medium as per the Lenz's law (Amjadian and Agrawal, 2020, 2018, 2017).

A large number of studies have focused on small sized EMEHs with single-frequency resonance which are referred to as narrow-band EMEHs. In these energy harvesters, the fundamental mode of vibration is usually tuned to resonate with the first significant frequency of the external excitation. The optimization of these types of EMEHs is limited to the components of the harvesting circuit (Beeby et al., 2007; El-hami et al., 2001; Elvin and Elvin, 2011; Halim et al., 2015; Kwon et al., 2013; Liu et al., 2015; Peigney and Siegert, 2020; Salauddin et al., 2016; Zeng and Khaligh, 2013). In the recent decade, a specific attention has been devoted to wide-band EMEHs in which the first several significant modes of vibration of the EMEH are tuned to resonate with the first several significant frequencies of the external excitation. Some examples are piecewiselinear harvester (Soliman et al., 2008), multi-frequency harvester with FR4 coils (Yang et al., 2009), locally resonant harvester (Mikoshiba et al., 2013), and multi-frequency harvester with magnetic spring (Foisal et al., 2012). The design of these types of EMEHs is complicated, and they are expensive to implement.

A scaling study has shown that, contrary to what commonly believed, the power density of an EMEH does not decrease proportionately with its volume as far as the electromechanical coupling remain strong (Arroyo et al., 2012). One of the effective methods to strengthen the electromechanical coupling in an EMEH is to optimize the arrangement of permanent magnets (PMs) poles in order to strengthen their magnetic field toward the copper coil. This research

project focuses on the design, modeling, and testing of a high-power EMEH consisting of PMs with linear pole arrangements. The objective of the study is to optimize the design of the EMEH such that it will be able to generate an average power of 1W and higher. This amount of electrical energy is sufficient to power conventional sensors installed on highway bridges with lowfrequency vibrations (Peigney and Siegert, 2020; Sazonov et al., 2009).

2.1: Electromechanical Model

Figure 2.1 shows the configuration of the EMEH consisting of a rectangular thick air-core copper coil (COIL) moving relative to two layers of three cuboidal permanent magnets (PMs) mounted on the left and right sides of the COIL. These PMs are attached to a firm base linked to the bridge that moves with the acceleration $\ddot{u}_{bX}(t)$ along the X-axis. The COIL is attached to this base through a thin flexible cantilever beam. The size of the horizontal air gap between the COIL and the left and right layers of PMs along the Z-axis is denoted by Δ_{gZ}, and the size of the air gap between the PMs along the X-axis is denoted by δ_{gX}.
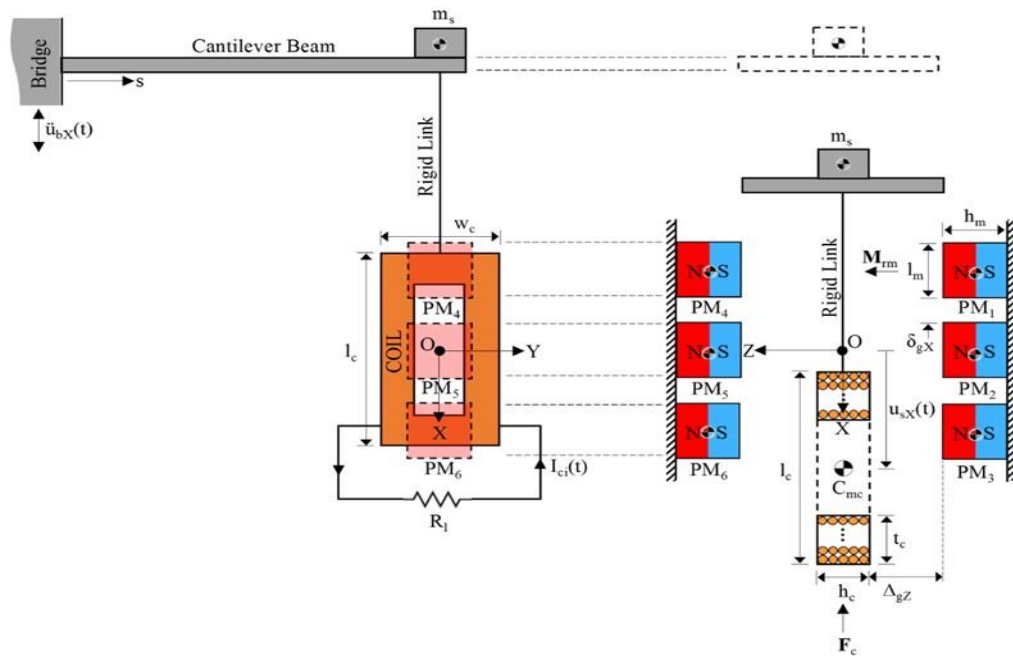
Figure 2.1. Configuration of the EMEH consisting of a cantilever beam, a rectangular thick aircore copper coil and two layers of three cuboidal permanent magnets.

The PMs are identical and each has the dimensions $l_m \times w_m \times h_m$. The dimensions of the left and right layers of PMs are then calculated to be $L_m = 3l_m + 2\delta_{gmx}$, $W_m = w_m$, and $H_m = h_m$. The COIL, as shown in Figure 1, has the dimensions $lc \times wc \times hc$, the winding depth t_c, and the total number of turns $N_c = N_z \times N_t$, where N_z and N_t are the numbers of turns along the Z-axis and the depth of the winding, respectively. It is ideally assumed that $N_z = h_c/d_w$ and $N_t = t_c/d_w$ where dw is the diameter of the winding wire made of copper. It is assumed that $I_{ci}(t) > 0$ when the electric current $I_{ci}(t)$ is counterclockwise in the XY-plane so that the N- and S-poles are established at $Z = +h_c/2$ and $Z = -h_c/2$, respectively, otherwise $I_{ci}(t) < 0$.
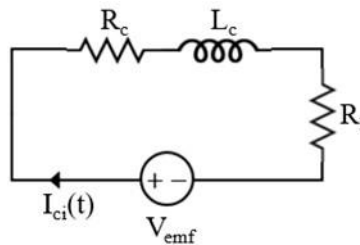
Figure 2.2. RL circuit model of the EMEH including an electric load with the resistance R_l.

A RL circuit consisting of a resistor with the resistance R_l (electrical load) connected to the COIL in series is used to harvest the electric power Pl from the EMEH as shown in Figure 2. Here, the COIL is represented by a resistor with the resistance R_c in series with an inductor with the induction L_c whose values are functions of the COIL's geometry. The electric power is generated by the electromagnetic induction occurring in the COIL when it moves relative to the PMs. This relative motion causes a change in the magnetic flux of the PMs passing through the COIL which induces the electromotive force V_{emf} in the circuit as per the Faraday's law of induction, and as a result,

the electric current $I_{ci}(t)$ is flowed through the COIL. It should be noted that the direction of this electric current changes as per the Lenz's law in such a way that the magnetic field of the COIL opposes the initial cause of change in the magnetic flux of the PMs which is the motion of the COIL. This magnetic interaction eventually excretes the magnetic force F_c on the COIL opposing to its motion, acting as a nonlinear braking/damping force.

2.1.1. Governing equation

The motion of the COIL through the magnetic field of the PMS when the beam is subjected to the base acceleration $\ddot{u}_{bx}(t)$ is described by the following coupled equations representing the electromechanical behavior of the system:

$$m_b \partial^2 w_b \partial t^2 (s,t) + c_b \partial w_b \partial t_\#(s,t) + E_b I_b \partial^4 w_b \partial s(\$s,t) = -m_b \ddot{u}_\#(t) \qquad (2.1)$$

$$L_\% dI_{\%\&} dt(t) + (R_' + R_\%) I_{\%\&}(t) = V_O^*(t) \qquad (2.2)$$

where, in Equation (2.1), mb and cb are the mass and mechanical damping per unit length of the beam, respectively, $E_b I_b$ is the flexural rigidity of the beam, and $w_b(s,t)$ is the transverse displacement of the beam along the X-axis relative to the base. The free end of the beam is subjected to force F_{cX} which is the X-component of the magnetic force F_c excreted on the COIL attached to the beam at s=L. This force and the tip (proof) mass ms representing the mass of the COIL and its associated components are taken into account by satisfying the force boundary condition at s=L (Erturk and Inman, 2008; Fu et al., 2019; Humar, 2012). The tip mass can be

increased to tune the fundamental frequency of the beam to the excitation frequency, thereby increasing the amplitude of the vibration and the output electrical power.

2.1.2. Electromechanical coupling coefficient

Equation (2.1) can be rewritten into the following form

$$F_{\%\#} = -K_* I_{\%\&} \tag{2.3}$$

where K_f is called electromechanical coupling coefficient or transformation factor (El-hami et al., 2001) that couples the mechanical domain to the electrical domain. This coefficient is time varying because the limits of integration in Equation (2.1) changes with the motion of the COIL. However, a quite large number of researchers (Beeby et al., 2007; Shen et al., 2018; Williams and Yates, 1996; Zhu et al., 2012; Zuo and Cui, 2013) have assumed that K_f is constant and does not change with time which is an oversimplified assumption that may lead to error in estimation of the harvested electric power (Cannarella et al., 2011; Mösch and Fischerauer, 2019). It can be also shown that,

$$V_{O^*} = \qquad\qquad +K_* \dot{u}_{+\#} \tag{2.4}$$

Equations (2.3) and (2.4) show that how the generation of the electromotive force Vemf (and the alternating current $I_{ci}=V_{emf}/(R_l+R_c)$) in the RL circuit is coupled to the velocity of the COIL and its magnetic interaction with the PMs.

2.1.3. SDOF model

It is more convenient to approximate the response of the cantilever beam with its response in the first mode of vibration which is in resonance with the external excitation. This approximation becomes more accurate when the tip mass is much larger than the total mass of the beam (Erturk and Inman, 2011, 2008). If we assume that $m_s/m_bL \to \infty$ then the governing equation can be written into the following form by eliminating $I_{ci}(t)$ from Equation (2.1) using Equations (2.3) and (2.4),

$$\ddot{u}_{sx}(t) + 2\xi_s\omega_s + \frac{K_f^2(t)}{2m_s\omega_s(R_{ci}+R_l)} + \dot{u}_{sx}(t) + \omega_s^2 u_{sx}(t) = \ddot{u}_{bx}(t) \tag{2.5}$$

where $\omega_s = 2\pi f_s$ is the natural circular frequency of the first mode of the beam in which f_s being the natural frequency, ξ_s is the critical mechanical damping ratio, and $u_{sx}(t)$ is the displacement of the free end of the beam or the COIL along the X-axis. This equation is nonlinear due to time variant nature of the electromechanical coupling coefficient $K_f(t)$. A numerical solver is used in SIMULINK ("Simulink 9.0," 2017) to solve it. The electrical power harvested from the EMEH is equal to the instantaneous power P_l consumed by the load, which is given by,

$$P_l(t) = R_l I_{ci}^2(t) \tag{2.6}$$

The parameter used to assess the performance of the EMEH is the average electrical power P_{lavg} given by the following integral taken over time interval [0, τ],

$$P_{\cdot -./} = \bar{\tau} \overset{1}{A_1} \overset{0}{P_{,}(t)} \, dt \qquad (2.7)$$

2.2. Parametric study

A parametric study is carried out in this section to optimize the configuration of the EMEH and its performance in harvesting electrical power from the traffic-induced vibration of highway bridges. The excitation of the base is assumed to be harmonic with the acceleration $\ddot{u}_{bx}(t)=\ddot{u}_{bXmax}\sin(2\pi f_b t)$ in which $\ddot{u}_{bXmax}$ and f_b are the amplitude and frequency, respectively. These parameters are set to $\ddot{u}_{bXmax}$=0.1g and f_b=4 Hz which are common values for highway bridges subjected to traffic loading (Peigney and Siegert, 2020). The response of the EMEH is a function of these parameters Δ_{gz}, δ_{gx}, l_c, w_c, h_c, t_c, d_w, l_m, w_m, h_m, B_{rm}, m_s, f_s, ξ_s, R_c, R_l, and τ. In this study, it is assumed that the PMs are cubic shaped with the size $l_m=w_m=h_m=a_m$=1 in and B_{rm}=1.4 T. It is further assumed that Δ_{gZ}=1/16 in, d_w=1 mm (18-AWG), R_c=2.173 Ω (for l_w=copper wire length=100 ft), m_s=704 gr (mass of the copper wire), f_s=4 Hz, ξ_s=0.05, and τ=1 sec. The rest of parameters including the dimensions of the COIL, δ_{gx}, and R_l referred to as optimization parameters (OPTPs) are varied to optimize the performance of the EMEH.

2.2.1. Dimensions of the COIL

The COIL is assumed to be cuboidal shaped with the length l_c, the width w_c, the height h_c, and the winding depth t_c. The length of the copper wire l_w winding the COIL is kept as a constant here that can be expressed in terms of the dimensions of the COIL as $l_w=2N_zN_t(l_c+w_c-2t_c)$. This expression is used to set up to following formula to find h_c in term of l_w, N_t, and d_w,

$$h_c = \frac{l_w^2}{2N_t^2 E(1+\alpha_c) GN_t d_w^2} l_w - 2l_c \qquad (2.8)$$

where $\alpha_c=w_c/l_c<1$ is the aspect ratio of the COIL on the XY-plane. It should be noted that $N_t<0.5\alpha_c(l_c/d_w)$ to make sure that the winding depth t_c remains less than the half of the width in accordance with the physics of the problem. The length of the COIL is fixed to be same as the length of the left and right PMs layers. This ensures that a minimal motion can cause the COIL to cut through the magnetic field of the PMs at the edges where the magnetic flux density varies sharply. The rest of OPTPs are assumed to have these values: $\delta_{gx}=1$ mm and $R_l=R_c=2.173$ Ω.
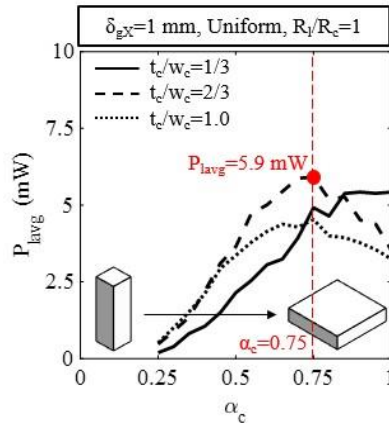
Figure 2.3. Effects of the geometry of the COIL on the harvested electrical power.

Figure 2.3 shows the variation of P_{lavg} with α_c for three different values of the winding depth: t_c/w_c=1/3, 2/3, and 3/3. It is seen that P_{lavg} increases with the increase of α_c implying that the more flatter the COIL, the higher electrical power can be harvested. The maximum harvested electrical power is equal to 5.9 mW that is obtained when α_c=0.75 and t_c/w_c=2/3 as illustrated in this figure. Therefore, the optimum dimensions of the COIL are l_c=3.079 in, w_c=2.309 in, h_c=1.048 in, and t_c=0.761 in.

2.2.1. Arrangement of the PMs

The arrangement of the PMs based on the direction of their poles and the size of the air gap between them can significantly affect their magnetic interaction with the COIL. Figure 2.4 shows two different arrangements of the PMs poles considered for evaluation of the EMEH in this study: (a) uniform and (b) alternating linear arrays. Figure 4(a) and (b) show the variation of P_{lavg} with δ_{gmX} when the PMs are arranged according to the uniform and alternating linear arrays,

respectively. The optimum dimensions of the COIL found in sub-section 3.1 have been used here with this assumption that $R_l=R_c=2.173\ \Omega$. Figure 2.5(a) shows that the variation of P_{lavg} with δ_{gmX} is harmonic-like for the uniform linear array, i.e. $P_{lavg}\sim\sin(\delta_{gmX})$. It first decreases and then increases as the thickness of the air gap between the PMs becomes larger. The maximum harvested electrical power is equal to 8.068 mW that is generated when $\delta_{gmX}=0.75$ in (red circle). Figure 2.5(b), however, shows that the variation of P_{lavg} with δ_{gmX} is bell-like for the alternating linear array. The maximum electrical power is calculated to be 269.4 mW which is remarkably larger than that calculated for the uniform linear array. This peak also happens when $\delta_{gmX}=3/4$ in (red circle). It is seen that at very large gaps $\delta_{gmX}>a_m=1$ in (black circle) the performances of both the linear arrays become similar as expected which is due to the fact that the magnetic interaction of the COIL with each PMs become independent from its magnetic interaction with other PMs. Therefore, the alternating linear array causes the highest amount of electrical power that can be harvested from the EMEH.
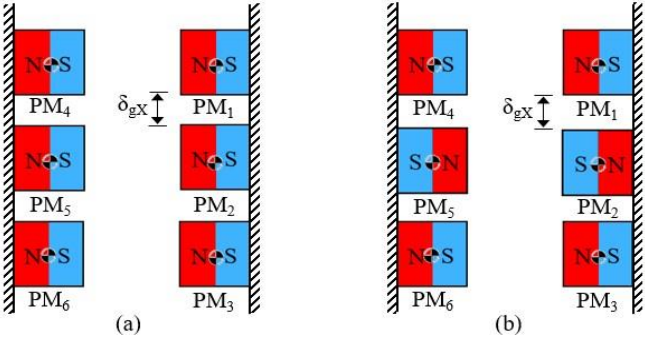

Figure 2.4. Two different arrangements of the PMs poles proposed for the design of the EMEH: (a) uniform and (b) alternating.
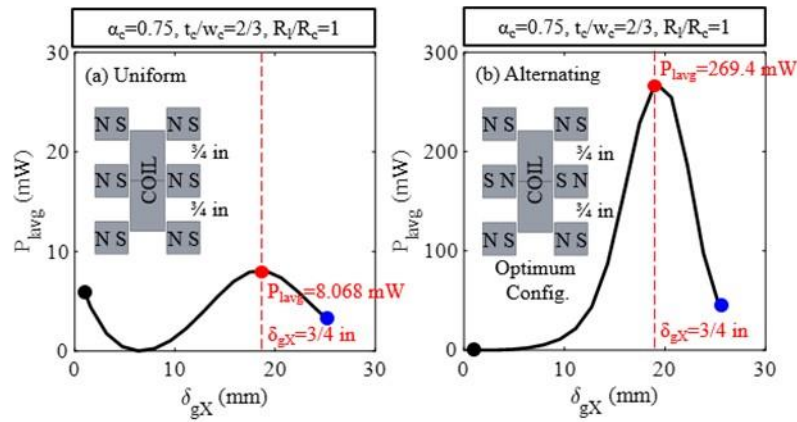
Figure 2.5. Effects of the arrangement of the PMs on the harvested electrical power: (a) uniform and (b) alternating linear arrays.

2.2.2. Electrical load

The electrical resistance of the harvesting circuit (electrical load) R_l can also significantly affect the performance of the EMEH and the amount of electrical power that can be extracted from it. This is a key parameter that can help to configure the electrical components of the harvesting circuit and its resultant resistance. Figure 2.6(a) shows the variation of P_{lavg} with R_l/R_c for the case when the PMs are arranged according to the alternating linear array with this assumption that δ_{gmX}=3/4 in. The optimum dimensions of the COIL found in sub-section 3.1 have been used here. It is seen that the maximum harvested electrical power is equal to 1716 mW that is obtained for R_l=0.25R_c=0.543 Ω or let say for a circuit with the equivalent electrical resistance of 0.5 Ω. It can also be seen that for R_l>R_c the harvested electrical power decreases dramatically which is due to this valid assumption that the electromechanical coupling coefficient K_f is a time-varying parameter. If we assume that K_f is constant and it does not change with time (Beeby et al., 2007; Shen et al., 2018; Williams and Yates, 1996; Zhu et al., 2012; Zuo and Cui, 2013) then the

maximum harvested electrical power is obtained when $R_l > R_c$ which is not consistent with the reality of the problem (Cannarella et al., 2011; Mösch and Fischerauer, 2019).

2.2.3. Base Excitation

The dynamic properties of the base acceleration including its amplitude and frequency can have significant effects on the performance of the EMEH. Figure 2.6(b) shows that to amplify the outputted electrical power it is essential to tune the fundamental frequency of the EMEH to the excitation frequency. A small decreasing in the peak acceleration of the traffic vibration from 0.1g to 0.075g (i.e., 25%) decreases the maximum electrical power from 1716 mW to 94.65 mW (i.e., 95 %), which is a significant reduction. This shows the importance of identification of the characteristics of the acceleration signal response of the target bridge before finalizing the design of the EMEH.
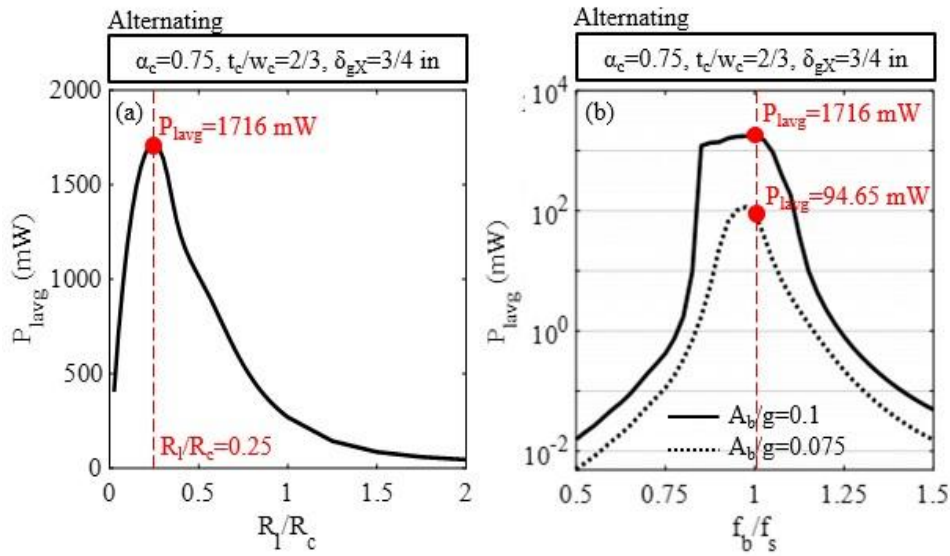
Figure 2.6. Effects of the (a) electrical resistance of the harvesting circuit and (b) dynamic characteristics of the traffic vibration on the harvested electrical power.

2.3. Numerical validation

A three-dimensional finite element (FE) model of the proposed EMEH is developed in COMSOL Multiphysics software (COMSOL v.5.4, 2018) to verify the accuracy of Equations (2) and (5). The configuration of the FE model has been optimized according to the results of the parametric analysis performed in section 3. Figures 2.7(a) shows this model and the details of the meshing. As can be seen a very fine mesh has been used along the edges of the COIL and PMs to achieve accurate results from the simulation. Figure 2.7(b) shows that the FE model is enclosed by a sphere of the radius r_a=6 in as the air domain whose center is positioned at the origin of the XYZ coordinate system which is located at the center of the air gap between the PMs. Figure 2.7(c) shows the magnetic flux density vector field of the PMs on the XZ-plane at Y=0 for u_{sX}=−0.322l_c and I_{ci}=−6.2 A.

Figures 2.8(a) to 2.8(c) show time histories of the displacement of the COIL u_{sX}, the induced electric current I_{ci}, and the magnetic force acting on the COIL F_{cX}, respectively. This force has been calculated from the analytical model for given values of u_{sX} and I_{ci} and will be compared to the corresponding results calculated from the FE model. Figures 2.8(a) and shows two points (red circle) chosen to calculate the magnetic force acting on the COIL where $u_{sX}=-0.322l_c$ and $+0.320l_c$, respectively. These displacements correspond to the electric currents $I_{ci}=-6.2$ A and -11.6 A, respectively, as illustrated on Figure 2.8(b). Figure 2.8(c) shows the values of the corresponding magnetic force F_{cX} acting on the COIL calculated from the FE model and then compared to the analytical model. It can be seen that there is a good agreement between both the models at both the points. This validates the accuracy of the analytical model developed to calculate the magnetic force using Equations (2) and (5).
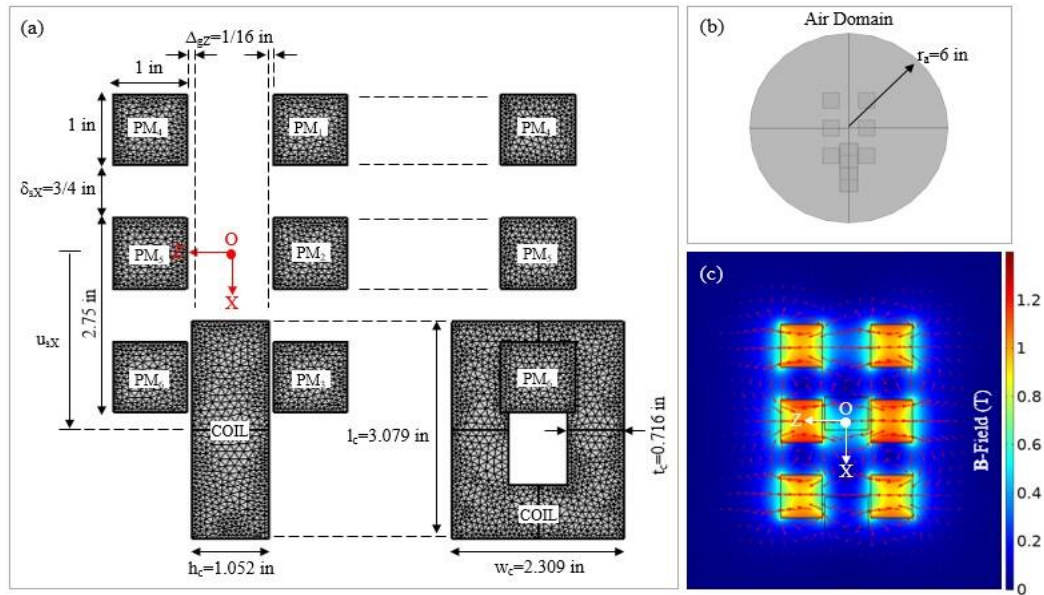
FIGURE 2.7 FE model of the EMEH developed in COMSOL: (a) meshing details, (b) air domain, and (c) magnetic flux density vector field of the PMs
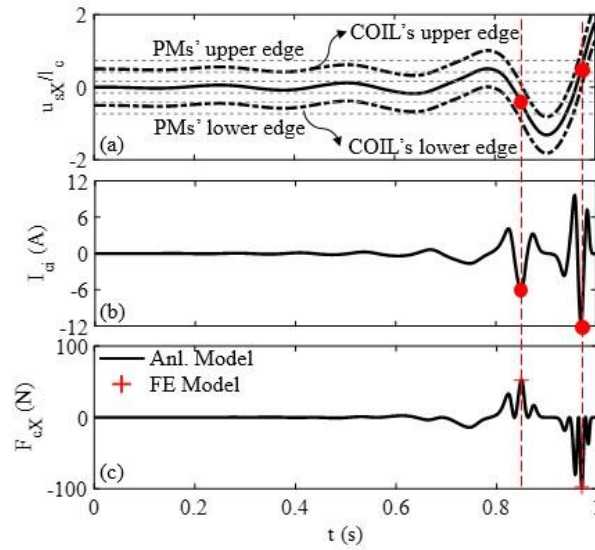

Figure 2.8 Comparison between the analytical model and the FE model to calculate the magnetic force; (a) displacement of the COIL, (b) electric current induced in the COIL, and (c) magnetic force F_{cX} acting on the COIL

Section 3: Design, Fabrication, And Laboratory Testing Of Proof-Of-The-Concept Prototype Of A Dual-Resonator Energy Harvester

3.1 Introduction

This chapter focuses on the design, fabrication, and laboratory testing of a proof-of concept prototype of a new EMEH with an optimized configuration. The design of this prototype, compared to the model studied in chapter 2, has been improved by adding one more resonator (cantilever beam) and more PMs.

3.2 Proof-of-the Concept Prototype

The benefit of using the strong electromechanical coupling between the moving coil (attached to the cantilever beam) and two layers of three PMs with alternating pole arrangements is further investigated by adding one more moving coil and one more layer of PMs with alternating pole arrangement to the energy harvester studied in chapter 2. This new energy harvester is termed as dual-resonator electromagnetic energy harvester (DR-EMEH) due to having two moving coils resonating with the base excitation or the bridge under the induced-vibration traffic.

Figure 3.1 shows the drawing details of the proof-of-the-concept prototype of proposed DREMEH with its key components and their geometrical parameters. This prototype consists of two rectangular copper coils of the size 1×0.5×1.5 in (and winding depth=0.375 in) attached to the free ends of two thin cantilever beams of the size 6×0.5×1/32 in vibrating with respect to three layers of neodymium PMs of the size 0.5×0.5×0.5 in with the magnetic remanence of B_{rm}=1.48 T (Neodymium, type N52). The other ends of cantilever beams, made of Aluminum, are fixed to

two separate Aluminum supports that can be moved to vary the length of the cantilever beams L_b. The neodymium PMs are attached to three Aluminum supports that with the cantilever beams supports sit on a thick Aluminum plate (rigid platform). Taking the maximum amplitude of the vibration of the copper coils into account, the amount of space the device occupies during its operation is about 6×3×4 in (V=0.001 m³).
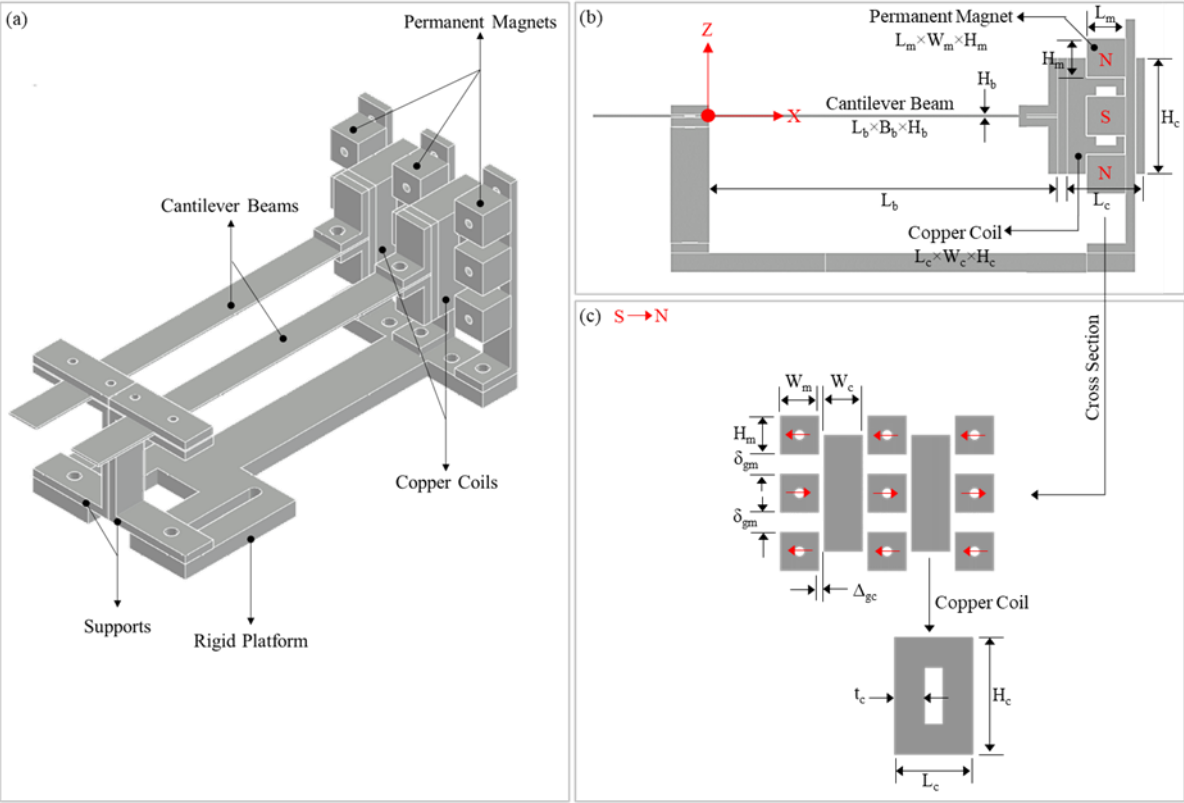

Figure 3.1. Drawing details of the dual-resonator energy harvester (a) 3D view, (b) longitudinal cross section with geometrical parameters, and (c) configuration of the PMs

Table 3.1 lists these parameters with their corresponding values as used for fabrication of the proof-of-the concept prototype. Here it should be noted that the two important parameters that have strong influence on the electrical power outputted from the device are: (1) the electromechanical coupling coefficient or transformation factor (El-hami et al., 2001) that is controlled by the pole arrangements of the PMs, and (2) the resonance frequency which is controlled by the length of the cantilever beams denoted by L_b in Figure 3.1(b). This length can be adjusted to tune the resonance frequency of energy harvester according to the predominant frequency of bridge at the location of the test. In this study, it is assumed that L_b=3 in and 4 in.

Table 3.1. Geometrical parameters of the key components of the DR-EMEH.

Parameter	Value	Unit	Description
L_b	Var.	in	The length of the cantilever beams
W_b	0.5	in	The width of the cantilever beams.
H_b	1/32	in	The thickness of the cantilever beams.
L_m	0.5	in	The length of the PMs.
W_m	0.5	in	The width of the PMs.
H_m	0.5	in	The thickness of the PMs.
L_c	1.0	in	The length of the copper coils.
W_c	0.5	in	The width of the copper coils.
H_c	1.5	in	The thickness of the copper coils.
t_c	0.375	in	The winding depth of the copper coils.
Δ_{gm}	5/64	in	The size of the gaps between the PMs and the copper coils.
δ_{gc}	3/8	in	The size of the gaps between the PMs in the Z-direction.

3.3. Laboratory Testing of the Prototype

The fabricated prototype of DR-EMEH was tested in the lab to evaluate its performance in generating electric voltage for the two arrangements of PMs introduced in chapter 2 as shown in Figure 2.4. Figure 3.2 shows the lab-bench setup established in the UTRGV Structural Engineering laboratory for testing the proof-of-the-concept prototype of the DR-EMEH under harmonic excitations. The apparatus used in this experiment are a an Electrodynamic Shaker (Vibration Research: VR5600, 110F-lb pk) used to simulate the harmonic excitation of base, a controller (Vibration Research: VR9500, 4 Channels, 24-bit Resolution) to control the shaker and record the acceleration and voltage data in the frequency domain, an accelerometer (PCB, 100 mV/g sensitivity, ±50 g pk) to measure the acceleration of the base, and a computer to processes the output signals.
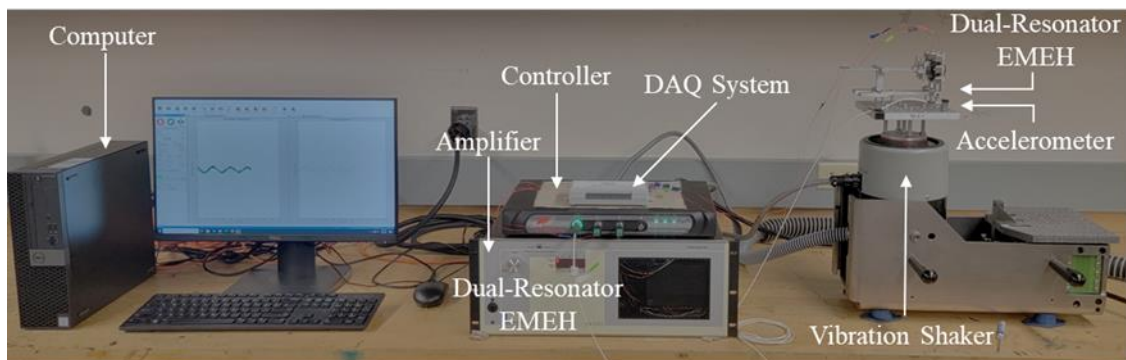

Figure 3.2. Experimental setup used to test the proof-of-concept prototype of the proposed DR-EMEH in a laboratory environment under harmonic excitations generated by an electromagnetic vibration shaker.
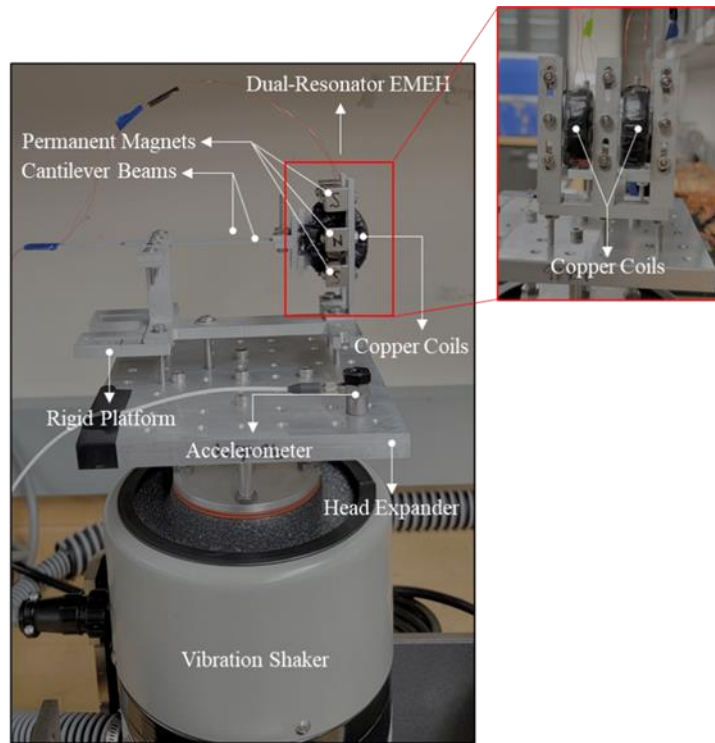
Figure 3.3. Testing of the proof-of-the-concept prototype of the proposed DR-EMEH; (a) 3D view of the fabricated device in laboratory with its key components, and (b) closeup view of the copper coils mounted on the free ends of cantilever beams (resonators).

Figure 3.3 shows the close-up view of mounting the DR-EMEH (with the PMs poles arranged alternately) on the vibration shaker. The accelerometer is installed on the head expander of the shaker to control the amplitude of input excitation and motion of the rigid platform beneath the DR-EMEH. The size of the air gaps between the PMs and the copper coils is about Δ_{gm}=5/64 in and the size of the air gaps between the PMs in the vertical direction is about δ_{gc}=3/8 in. The performance of DR-EMEH is evaluated under a linear sin sweep frequency test in which the acceleration of the vibration shaker is,

$$\ddot{u}_! = A_! sin\ E2\pi\ Nf_, + \underline{\quad\quad} f" t^-{}_4{}^f{}_, tP\ tI \tag{3.1}$$

where f_1=2.5 Hz, f_2=22.5 Hz and t_n=60 sec. The amplitude of traffic-induced acceleration of a highway bridge under a common daily traffic is usually less than 0.1g, for this reason it is assumed that A_b={0.05g, 0.075g, 0.1g}. In this study, the harvested voltage is open circuit implying that the voltage is measured without connecting the DR-EMEH to any middle circuit.

Figure 3.4 shows the voltages outputted from the resonator 1 and 2 of DR-EMEH with uniform pole arrangement plotted versus the frequency of the base excitation. Figure 3.4(c) shows that the maximum voltage harvested is about 0.7 V for both the resonators when A_b=0.1g. This voltage is measured at a resonance frequency band ranging from f=7 Hz to 8 Hz. Figure 3.5 shows the time histories of the voltages output from these two resonators for A_b=0.1g. Figure 3.6 shows the voltages outputted from the resonator 1 and 2 of DR-EMEH with alternating pole arrangement plotted versus the frequency of the base excitation. The resonance frequency of resonators 1 and 2 are measured to be f=7.6 Hz and f=7.8 Hz, respectively.
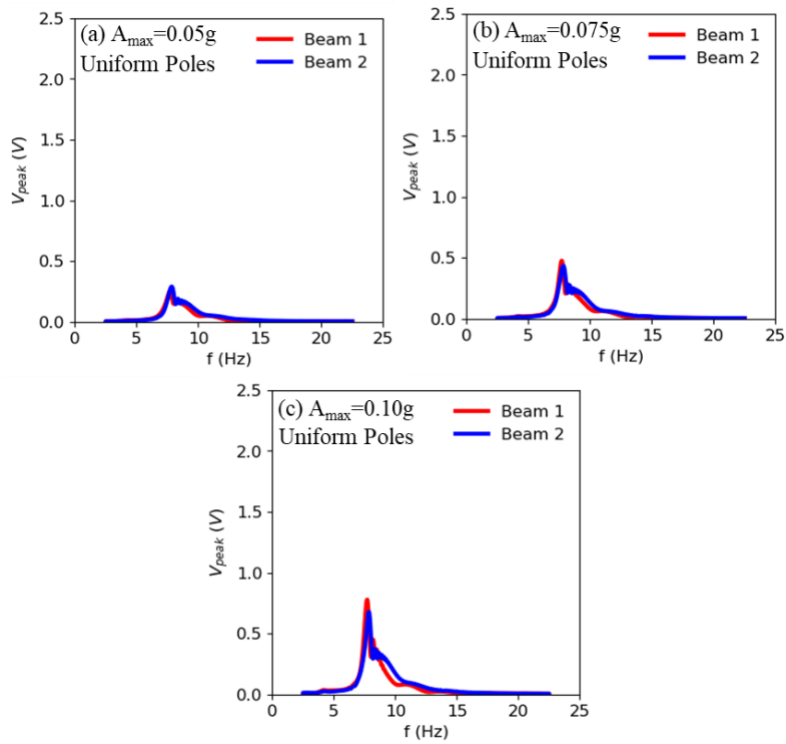
Figure 3.4. Voltage outputted from the DR-EMEH with uniform pole arrangement plotted versus the frequency of the base excitation for (a) A_b=0.05g, (d) A_b=0.075g, (c) A_b=0.1g.

Figure 3.5. Time-histories of voltage outputted from the DR-EMEH with uniform pole arrangement plotted for A_b=0.1g, (a) Resonator 1 and (2) Resonator 2.

Figure 3.6. Voltage outputted from the DR-EMEH with alternating pole arrangement plotted versus the frequency of the base excitation for (a) A_b=0.05g, (d) A_b=0.075g, (c) A_b=0.1g.
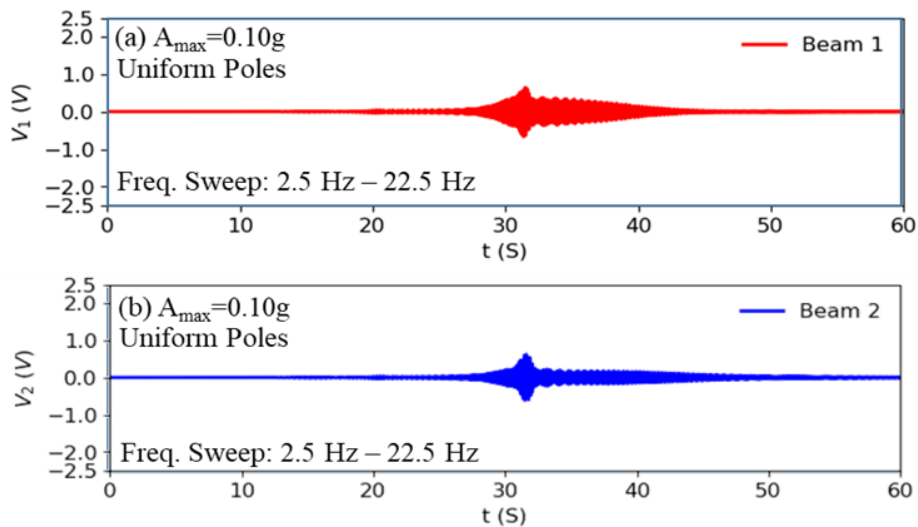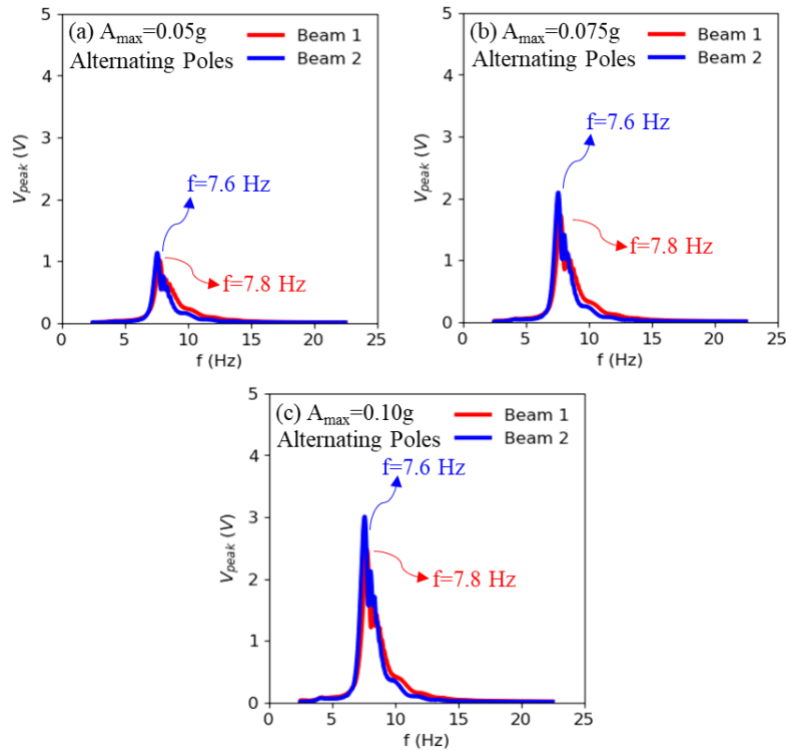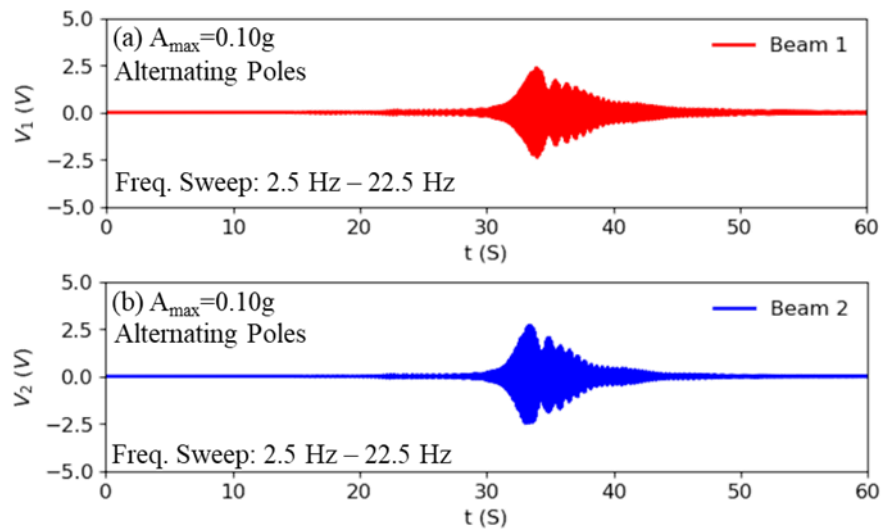

Figure 3.7. Time-histories of voltage outputted from the DR-EMEH with alternating pole arrangement plotted for Ab=0.1g, (a) Resonator 1 and (2) Resonator 2.

Figure 3.6(c) shows that for A_b=0.1g the maximum voltage harvested from the device is about 3.0 V for both the resonators at their resonance frequencies. This shows that the amount of voltage harvested from the device with the alternating pole arrangement can be 4 times higher than in the case when the PMs poles have a uniform arrangement. Figure 3.7 shows the time histories of the voltages output from the resonators 1 and 2 for A_b=0.1g. The amplified voltage response shown from t=30 sec to t=40 sec corresponds to the resonance of the device with the base excitation.

Section 4: Field Testing Of The Dual-Resonator Energy Harvester

The performance of proof-of-the-concept prototype of the DR-EMEH was further investigated by conducting a field-testing study to install DR-EMEH on three highway bridges over the Passaic River in New Jersey. Figure 4.1. shows the locations of these bridges on the Google map: (1) Hillery Street bridge, (2) De Jessa Memorial Bridge, and (3) Main Avenue Bridge. These bridges were tested during the rush hours when the traffic load was relatively heavier.
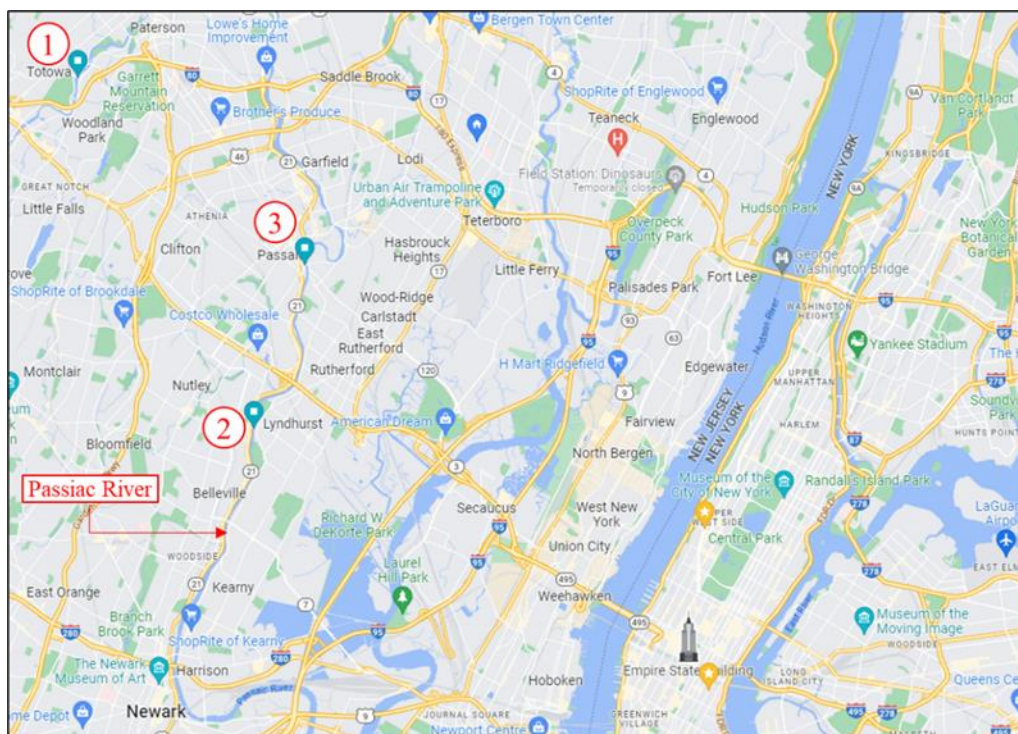
Figure 4.1. Locations of the highway bridges on the Google map: (1) Hillery Street bridge, (2) De Jessa Memorial Bridge, and (3) Main Avenue Bridge.

4.1. Hillery Street Bridge

The Hillery Street Bridge is a three-span Pratt pony steel truss bridge over the Passaic River in Totowa and Woodland Park, New Jersey. The bridge was initially constructed in 1898 and underwent rehabilitation in 1973. In 2009, it was extensively renovated to restore its original historical state, including its lattice-work sidewalk railings.

Figure 4.2. Field testing of the DR-EMEH on the Hillery Street Bridge in NJ: (a) photo of the bridge taken from the Google map with the location of testing marked, (b) testing setup, and (c) mounting of the device on the railing of bridge sidewalk.

Figure 4.2 shows the installation of the device on Hillery Street Bridge. The device was safely mounted on the railing of bridge sidewalk using electrical tape at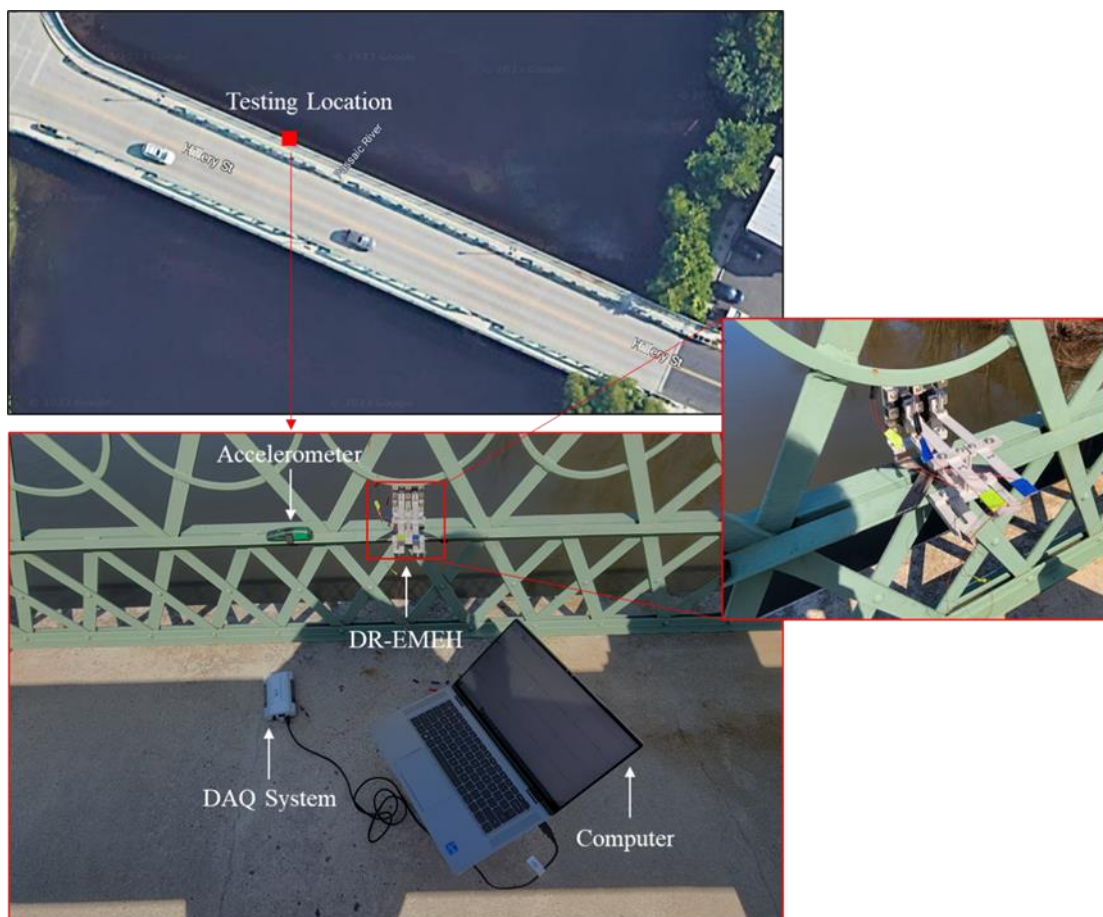 a location close to mid of the bridge span (See Figure 4.2(a)). In this test, Lb=3 in for both the resonators. In addition, an accelerometer was installed on the railing at a location very close to the device to measure the acceleration of the bridge during the testing. The harvested voltage was recorded using a DAQ system connected to a computer (Laptop) in the field as shown in Figure 4.2(b).

Figure 4.3(a) shows the time history of the acceleration of the bridge recorded during the test. The peak value of the acceleration is less than 0.05g. Figure 4.3(b) shows the power spectral density of the acceleration signal containing several peaks representing the dominant frequency of the bridge itself and the moving load during the test. Figure 4.4 shows the time histories of voltages harvested from the vibration of resonators 1 and 2 during a 10-minute test. The peak value of the voltage for resonator 1 is less than 0.05V which is very low due to the low amplitude of bridge acceleration and mistuning of the device frequency with the dominant frequency of the bridge and the moving load.
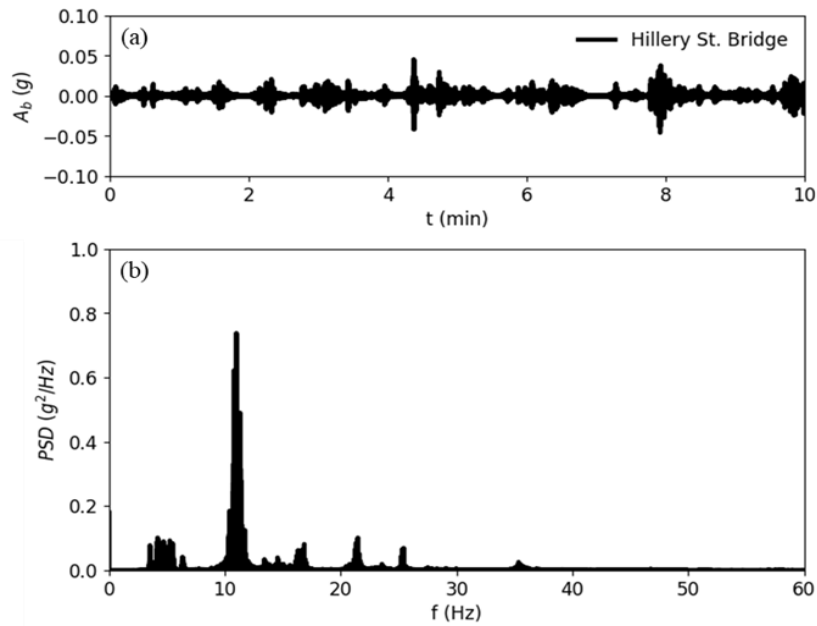
Figure 4.3. Acceleration response of the Hillery Street Bridge during the test: (a) time-history and (b) power-spectral density
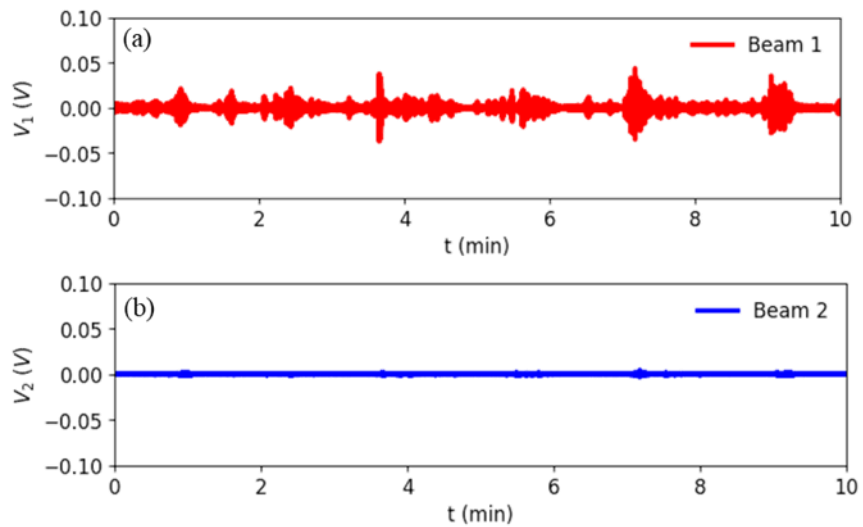

Figure 4.4. Time history of voltage harvested from the traffic-induced vibration of the Hillery Street Bridge: (a) resonator 1 and (b) resonator 2.

4.2. De Jessa Memorial Bridge

De Jessa Memorial Bridge (also known as Kingsland Avenue Bridge) is a four-span Warren pony steel truss bridge over the Passaic River that connects the Township of Lyndhurst to the Township of Nutley in New Jersey. The bridge is old, was initially built in 1905 and then partially renovated in 1986. The bridge, which is more than a century old, is now deemed functionally obsolete due to its incapability to accommodate current traffic demands, considering its load-carrying capacity and deck geometry (Source: https://www.kingslandavenuebridge.com/faq/). This implies that if redesigned, the bridge can carry a higher volume of traffic that can result in higher harvested electric power during rush hours.

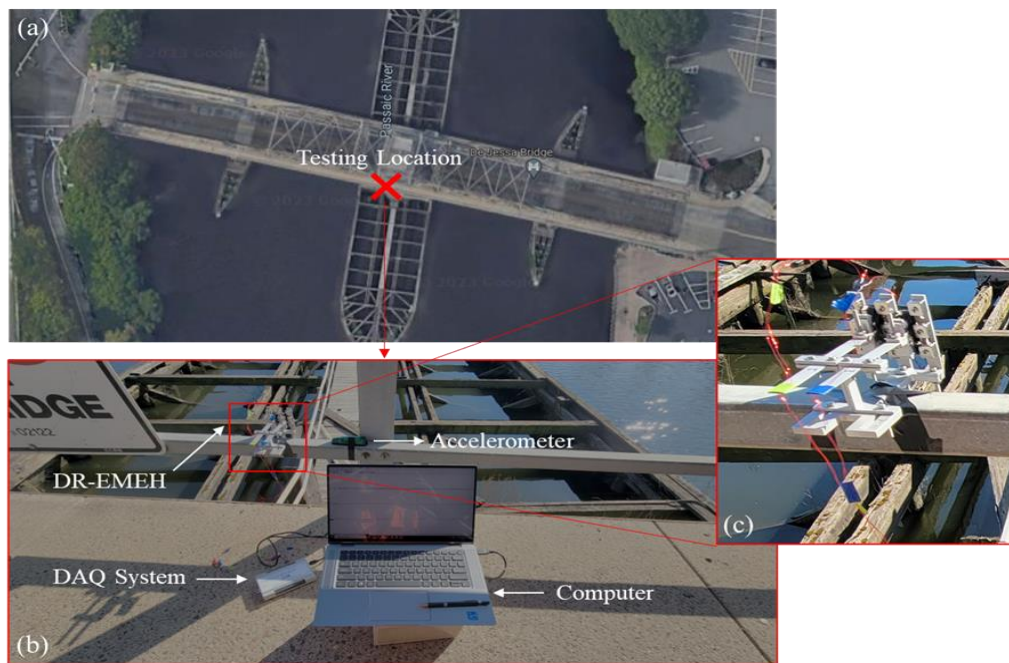

Figure 4.5. Field testing of the DR-EMEH on the De Jessa Memorial Bridge in NJ: (a) photo of the bridge taken from the Google map with the location of testing marked, (b) testing setup, and (c) mounting of the device on the sidewalk railing.

Figure 4.5 shows the installation of the device on the De Jessa Memorial Bridge in a point very close the midpoint of span. The device was safely mounted on the railing of bridge sidewalk using electrical tape to harvest the voltage for 10 minutes (See Figure 4.5(a)). Likewise, in this test, Lb=3 in for both the resonators. The accelerometer was installed on the railing at a location very close to the device to measure the acceleration of the bridge during the testing. The harvested voltage was recorded using a DAQ system connected to a computer (Laptop) in the field as shown in Figure 4.5(b).

Figure 4.6(a) shows the time history of the acceleration of the bridge recorded during the test for 10 minutes. For this bridge, the peak value of the acceleration was less than 0.15g, that is almost three times of the peak acceleration recorded on the Hillery Street Bridge. Figure 4.3(b) shows the power spectral density of the acceleration signal containing several peaks representing the dominant frequency of the bridge itself and the moving load during the test. Figure 4.7 shows the time histories of voltages harvested from the vibration of resonators 1 and 2 during the test. The peak value of the voltage for resonator 1 is less than 0.15V. This amount of voltage is low, which just like the Hillery Street Bridge, is due to the low amplitude of bridge acceleration and mistuning of the device frequency with the dominant frequency of the bridge and the moving load.

Figure 4.6. Acceleration response of the De Jessa Memorial Bridge during the test: (a) timehistory and (b) power-spectral density.

Figure 4.7. Time history of voltage harvested from the traffic-induced vibration of the De Jessa Memorial Bridge: (a) resonator 1 and (b) resonator 2.

4.3. Main Avenue Bridge

The Main Avenue Bridge (or Gregory Avenue Bridge) is a three-span Thru steel truss bridge carrying a 2-lane street with sidewalks over the Passaic River in Passaic & Wallington, New Jersey. The bridge was constructed in 1906 and underwent some rehabilitations and changes in 1985.
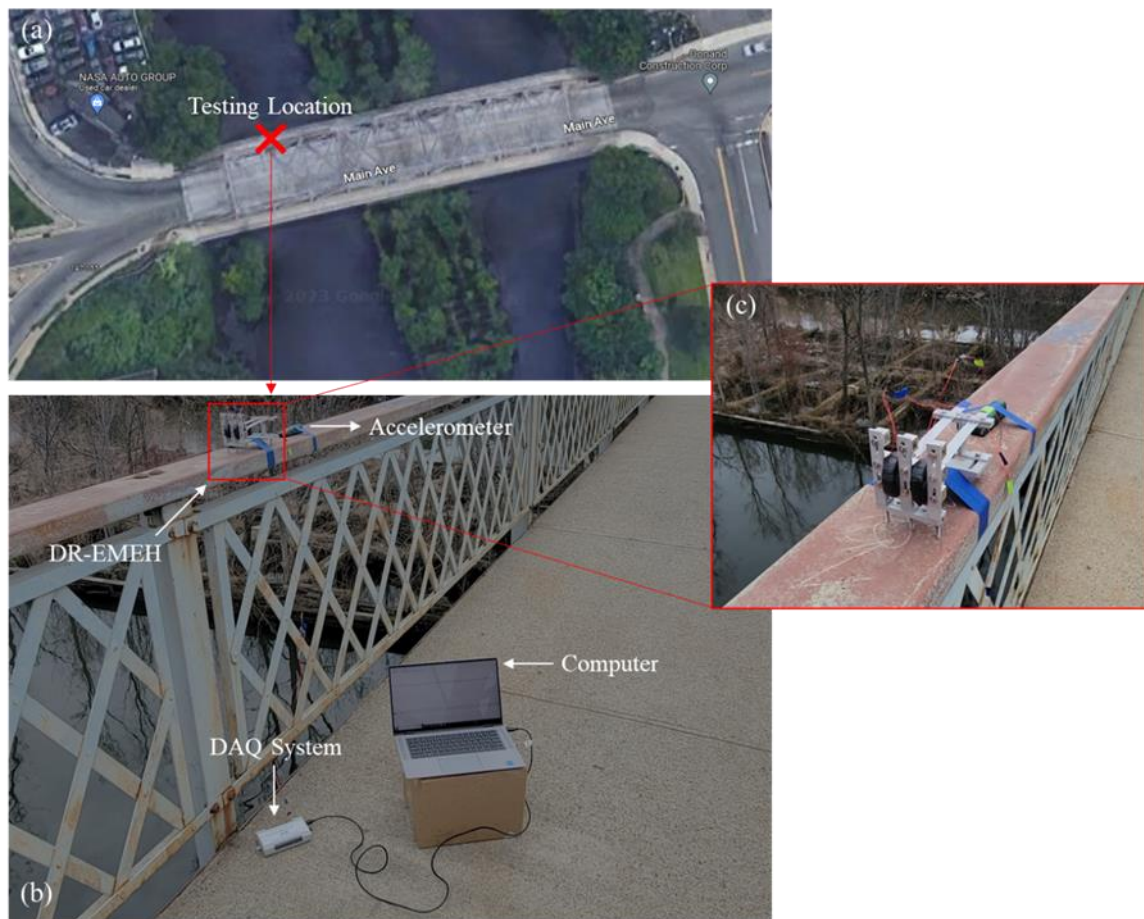
Figure 4.8. Field testing of the DR-EMEH on the Main Avenue Bridge in NJ: (a) photo of the bridge taken from the Google map with the location of testing marked, (b) testing setup, and (c) mounting of the device on the sidewalk railing.

Figure 4.8 shows the installation of the DR-EMEH on the Main Avenue Bridge. As can be seen, the device was installed in the middle of the third span where the amplitude of vibration was measured to be relatively high. Figure 4.8(b) and (c) show that the device was mounted on the railing of bridge sidewalk using electrical tape. The test was run for 10 minutes. However, in contrast to the previous two tests, in this test L_b was set to be 4 in for both the resonators resulted in the reduction of the frequency of resonators from f=7.5 Hz to f=5.5 Hz. Figure 4.8(b) also shows that the accelerometer was installed on the railing at a location very close to the device to measure the acceleration of the bridge during the testing. Like the prior two tests, the harvested voltage was recorded using a DAQ system connected to a computer (Laptop) on the bridge as shown in Figure 4.5(b).

Figure 4.9(a) shows the time history of the acceleration of the bridge recorded during the test for 10 minutes. The peak value of the acceleration is about 0.1g. Figure 4.9(b) shows the power spectral density of the acceleration signal that includes several peaks ranging from 5 Hz to 40 Hz representing the dominant frequency of the bridge itself and that of the moving load during the test. Figure 4.7 shows the time histories of voltages harvested from the vibration of resonators 1 and 2 during the test where L_b=4 in. The peak value of the voltage for resonator 1 is about 0.75 V and for resonator 2 is about 1.25 V, which are much larger than those recorded for the two prior highway bridges.
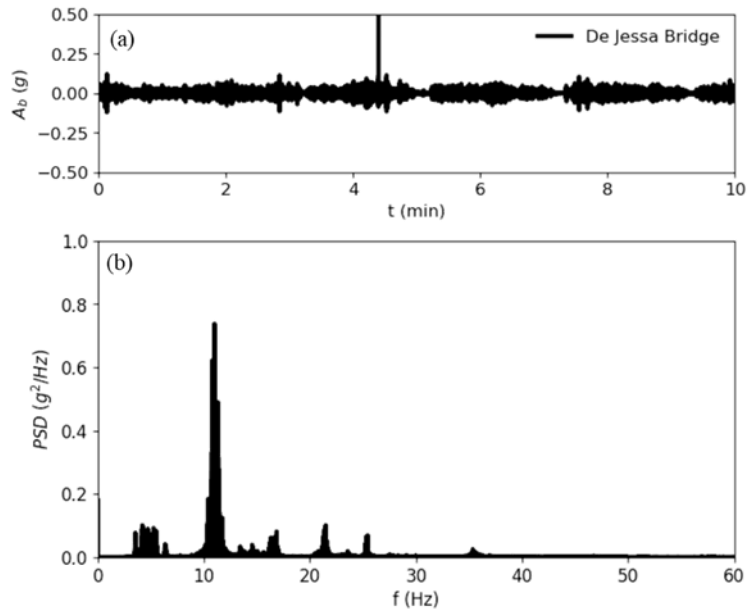
Figure 4.9. Acceleration response of the Main Avenue Bridge during the test: (a) time-history and (b) power-spectral density.

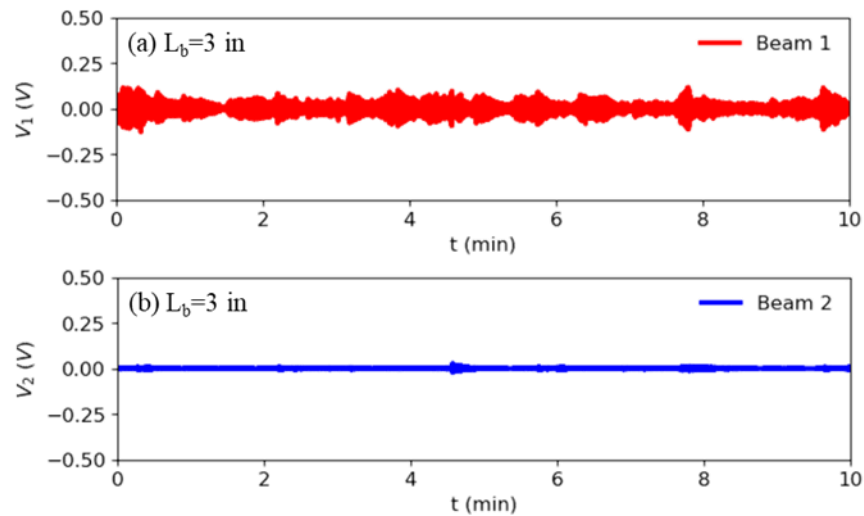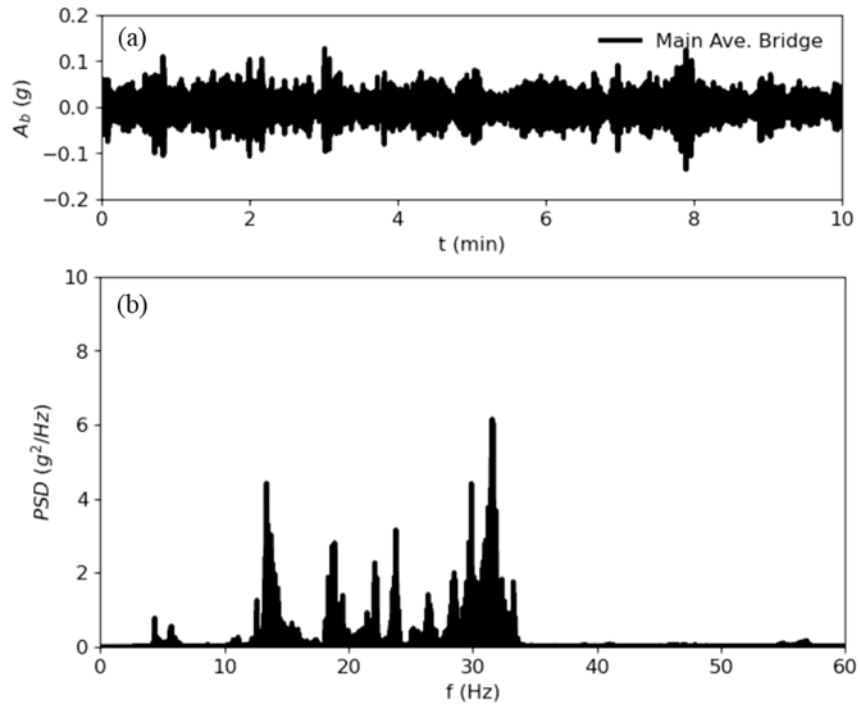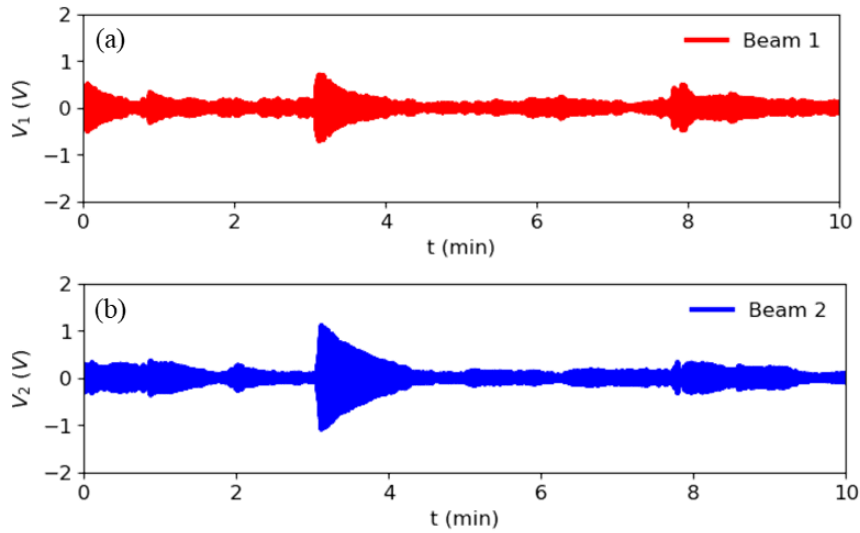**Figure 4.10.** Time history of voltage harvested from the traffic-induced vibration of the Main Avenue Bridge: (a) resonator 1 and (b) resonator 2.

Section 5. Conclusions

This report focuses on the design (optimization), fabrication, and testing of a high-power narrow band EMEH to be able to generate an average electrical power of about 500 mW and more at the resonance frequency. This amount of electrical energy alone is more than enough to power conventional wireless sensors used for their structural health monitoring. The results of this research yielded several notable conclusions, some of which are listed below:

1. First, an analytical model was developed to optimize a simple model of an EMEH with linear arrays of PMs. The proposed EMEH consists of two stationary layers of three cuboidal neodymium PMs, a rectangular thick air-core copper coil (copper coil) attached to the free end of a flexible cantilever beam whose fixed end is firmly attached to the highway bridge oscillating in the vertical motion due to passing traffic. An analytical model has been developed to conduct a parametric study and optimize the geometry of the copper coil, the arrangement of the PMs, and the resistance of the harvesting circuit. This analytical model has been validated by a FE simulation in COMSOL.

2. It has been shown that arranging the PMs in an alternating layout can significantly increase the generated power if the thickness of the air gap between the PMs to be large enough to amplify the magnetic interaction between the PMs. The numerical results show that the maximum harvested electrical power is equal to 1716 mW obtained by a harvesting circuit with an electrical resistance of 0.5 Ω.

3. Second, an enhanced model of the EMEH (dual-resonator EMEH) was designed and fabricated for laboratory and field tests. This prototype consists of two rectangular copper coils of the size 1×0.5×1.5 in (and winding depth=0.375 in) attached to the free ends of two thin cantilever beams of the size 6×0.5×1/32 in vibrating with respect to three layers of cuboidal neodymium PMs of the size 0.5×0.5×0.5 in with the magnetic remanence of B_{rm}=1.48 T.

4. The results of laboratory test showed that each of the resonators in the DR-EMEH can generate a voltage up to 3V for a resonance frequency about 7.7 Hz under a harmonic acceleration with the amplitude 0.1g. The results of field test showed that the performance of the DR-EMEH is significantly affected by the frequency of moving load, and if necessary, it needs to be redesigned according to the dominant frequency of moving load during rush hour.

5. It is worth mentioning that the main drawback of the proposed EMEH is its large vibration amplitude that limits its field application. A mechanical stopper can be installed to limit the amplitude of the copper coil, although this to some extent may limit the amount of output electrical power due to impact.

References

Amjadian, M., Agrawal, A.K., 2020. Planar Arrangement of Permanent Magnets in Design of a MagnetoSolid Damper by Finite Element Method. Journal of Intelligent Material Systems and Structures.

Amjadian, M., Agrawal, A.K., 2018. Modeling, design, and testing of a proof-of-concept prototype damper with friction and eddy current damping effects. Journal of Sound and Vibration 413, 225–249. https://doi.org/10.1016/j.jsv.2017.10.025

Amjadian, M., Agrawal, A.K., 2017. A passive electromagnetic eddy current friction damper (PEMECFD): Theoretical and analytical modeling. Structural Control and Health Monitoring 24, e1978. https://doi.org/10.1002/stc.1978

Arroyo, E., Badel, A., Formosa, F., Wu, Y., Qiu, J., 2012. Comparison of electromagnetic and piezoelectric vibration energy harvesters: Model and experiments. Sensors and Actuators, A: Physical 183, 148–156. https://doi.org/10.1016/j.sna.2012.04.033

Beeby, S.P., Torah, R.N., Tudor, M.J., Glynne-Jones, P., O'Donnell, T., Saha, C.R., Roy, S., 2007. A micro electromagnetic generator for vibration energy harvesting. Journal of Micromechanics and Microengineering 17, 1257–1265. https://doi.org/10.1088/0960-1317/17/7/007

Cannarella, J., Selvaggi, J., Salon, S., Tichy, J., Borca-Tasciuc, D.A., 2011. Coupling factor between the magnetic and mechanical energy domains in electromagnetic power harvesting applications. IEEE Transactions on Magnetics 47, 2076–2080. https://doi.org/10.1109/TMAG.2011.2122265 COMSOL v.5.4, 2018. Multiphysics® Modeling Software v.5.4.

El-hami, M., Glynne-Jones, P., White, N.M., Hill, M., Beeby, S., James, E., Brown, A.D., Ross, J.N., 2001. Design and fabrication of a new vibration-based electromechanical power generator. Sensors and Actuators, A: Physical 92, 335–342. https://doi.org/10.1016/S0924-4247(01)00569-6

Elvin, N.G., Elvin, A.A., 2011. An experimentally validated electromagnetic energy harvester, in: Journal of Sound and Vibration. Academic Press, pp. 2314–2324. https://doi.org/10.1016/j.jsv.2010.11.024

Erturk, A., Inman, D.J., 2011. Piezoelectric Energy Harvesting, Piezoelectric Energy Harvesting. John Wiley & Sons, Ltd, Chichester, UK. https://doi.org/10.1002/9781119991151

Erturk, A., Inman, D.J., 2008. On Mechanical Modeling of Cantilevered Piezoelectric Vibration Energy Harvesters. Journal of Intelligent Material Systems and Structures 19, 1311–1325. https://doi.org/10.1177/1045389X07085639

Foisal, A.R.M., Hong, C., Chung, G.S., 2012. Multi-frequency electromagnetic energy harvester using a magnetic spring cantilever. Sensors and Actuators, A: Physical 182, 106–113. https://doi.org/10.1016/j.sna.2012.05.009

Fu, Y., Ouyang, H., Davis, R.B., 2019. Triboelectric energy harvesting from the vibro-impact of three cantilevered beams. Mechanical Systems and Signal Processing 121, 509–531. https://doi.org/10.1016/j.ymssp.2018.11.043

Halim, M.A., Cho, H., Park, J.Y., 2015. Design and experiment of a human-limb driven, frequency upconverted electromagnetic energy harvester. Energy Conversion and Management 106, 393–404.
https://doi.org/10.1016/j.enconman.2015.09.065

Humar, J., 2012. Dynamics of Structures, 3rd ed. CRC Press.

Jia, Y., 2020. Review of nonlinear vibration energy harvesting: Duffing, bistability, parametric, stochastic and others. Journal of Intelligent Material Systems and Structures 31, 921–944. https://doi.org/10.1177/1045389X20905989

Khaligh, A., Zeng, P., Zheng, C., 2010. Kinetic energy harvesting using piezoelectric and electromagnetic technologiesstate of the art. IEEE Transactions on Industrial Electronics 57, 850–860. https://doi.org/10.1109/TIE.2009.2024652

Kwon, S.-D., Park, J., Law, K., 2013. Electromagnetic energy harvester with repulsively stacked multilayer magnets for low frequency vibrations. Smart Materials and Structures 22, 055007. https://doi.org/10.1088/0964-1726/22/5/055007

Liu, X., Qiu, J., Chen, H., Xu, X., Wen, Y., Li, P., 2015. Design and Optimization of an Electromagnetic Vibration Energy Harvester Using Dual Halbach Arrays. IEEE Transactions on Magnetics 51. https://doi.org/10.1109/TMAG.2015.2437892

Mikoshiba, K., Manimala, J.M., Sun, C., 2013. Energy harvesting using an array of multifunctional resonators. Journal of Intelligent Material Systems and Structures 24, 168–179.

https://doi.org/10.1177/1045389X12460335

Mösch, M., Fischerauer, G., 2019. A Comparison of Methods to Measure the Coupling Coefficient of Electromagnetic Vibration Energy Harvesters. Micromachines 10, 826. https://doi.org/10.3390/mi10120826

Peigney, M., Siegert, D., 2020. Low-Frequency Electromagnetic Energy Harvesting from Highway Bridge Vibrations. Journal of Bridge Engineering 25, 04020056. https://doi.org/10.1061/(ASCE)BE.19435592.0001581

Priya, S., Inman, D.J., 2009. Energy harvesting technologies, Energy Harvesting Technologies. Springer US. https://doi.org/10.1007/978-0-387-76464-1

Roundy, S., Wright, P.K., Rabaey, J.M., 2004. Energy Scavenging for Wireless Sensor Networks, Energy Scavenging for Wireless Sensor Networks. Springer US. https://doi.org/10.1007/978-1-46150485-6

Salauddin, M., Halim, M.A., Park, J.Y., 2016. A magnetic-spring-based, low-frequency-vibration energy harvester comprising a dual Halbach array. Smart Materials and Structures 25, 095017. https://doi.org/10.1088/0964-1726/25/9/095017

Sazonov, E., Pillay, P., Li, H., Curry, D., 2009. Self-Powered Sensors for Monitoring of Highway Bridges. IEEE Sensors Journal 9, 1422–1429. https://doi.org/10.1109/JSEN.2009.2019333

Shen, W., Zhu, S., Xu, Y.-L., Zhu, H., 2018. Energy regenerative tuned mass dampers in high-rise buildings. Structural Control and Health Monitoring 25, e2072. https://doi.org/10.1002/stc.2072 Simulink 9.0, 2017.

Soliman, M.S.M., Abdel-Rahman, E.M., El-Saadany, E.F., Mansour, R.R., 2008. A wideband vibration-based energy harvester. Journal of Micromechanics and Microengineering 18. https://doi.org/10.1088/0960-1317/18/11/115021

Wei, C., Jing, X., 2017. A comprehensive review on vibration energy harvesting: Modelling and realization. Renewable and Sustainable Energy Reviews. https://doi.org/10.1016/j.rser.2017.01.073

Williams, C.B., Yates, R.B., 1996. Analysis of a micro-electric generator for microsystems. Sensors and Actuators, A: Physical 52, 8–11. https://doi.org/10.1016/0924-4247(96)80118-X

Zeng, P., Khaligh, A., 2013. A permanent-magnet linear motion driven kinetic energy harvester. IEEE Transactions on Industrial Electronics 60, 5737–5746. https://doi.org/10.1109/TIE.2012.2229674

Zhu, S., Shen, W. ai, Xu, Y. lin, 2012. Linear electromagnetic devices for vibration damping and energy harvesting: Modeling and testing. Engineering Structures 34, 198–212. https://doi.org/10.1016/j.engstruct.2011.09.024

Zuo, L., Cui, W., 2013. Dual-functional energy-harvesting and vibration control: Electromagnetic resonant shunt series tuned mass dampers. Journal of Vibration and Acoustics, Transactions of the ASME 135. https://doi.org/10.1115/1.4024095